Solution pK_a Values of the Green Fluorescent Protein Chromophore from Hybrid Quantum-Classical Calculations

Christina Scharnagl*,† and Robert A. Raupp-Kossmann‡

Physik-Department, E14 Lehrstuhl für Physik Weihenstephan, Technische Universität München, D-85350 Freising, Germany, and Institut für Theoretische Physik T38, Technische Universität München, D-85747 Garching, Germany

Received: August 13, 2003; In Final Form: October 28, 2003

We present a theoretical study of the four aqueous microscopic dissociation constants relating the relevant protonation forms (cation, neutral, anion, zwitterion) of the chromophore of the green fluorescent protein (GFP) in the ground and excited states. To take the protonation-state-dependent torsional flexibility around the ring-bridging bonds into account, configuration integrals in the torsion space were evaluated to yield the free energy differences. Conformational energies were calculated within a semiempirical quantum chemical scheme using a continuum solvation model. After establishing a linear regression of experimental aqueous pK_a's and calculated enthalpy differences for a series of reference molecules with phenolic hydroxyl or imino nitrogen, the applied method is able to reproduce the titration behavior of bifunctional groups within an average error of 0.8 pK-units. The calculated values for the GFP chromophore agree very well (deviation $<$ 0.2 pK-units) with known ground-state aqueous pK_a's and confirm the equilibrium between neutral and anionic forms (pK_a = 8.3). Freezing torsional flexibility shifts this pK_a to 6.6—in accordance with entropic contributions due to the enlarged configurational space of the protonated compound—and is, therefore, a dominant contribution to the adjustment of pK_a's in the protein. Estimates for the excited-state pK_a's were derived from vertical excitation energies under the assumption that the protolytic equilibria are faster than conformational relaxation of solute and solvent—corresponding to a recent experimental model of excited-state proton transfer in GFP. The calculations reveal that increase of both the acidity of the phenolic oxygen and the basicity of the heterocycle nitrogen works in synergy. The neutral form becomes a strong photoacid and transfers a proton with a pK_a* = 0.1; the imino-N becomes a strong photobase capable of accepting a proton with a pK_a* = 8.9. Provided an extended hydrogen-bonded network links the two functions, phototautomerization might be a possible decay pathway.

1. Introduction

Due to its intrinsic fluorophore, green fluorescent protein (GFP) has found widespread use as a label in biophysical and biochemical investigations.[1] The chromophore, 4-hydroxybenzylidene-imidazolinone (abbreviated in this study as HBI, Figure 1), is formed in an autocatalytic post-translational cyclization, dehydration, and oxidation of three internal residues Ser65−Tyr66−Gly67.[2] It consists of a conjugated π-system connecting the phenol ring from Tyr66 with the imidazolinone heterocycle derived from the backbone cyclization of residues 65 and 67. As shown by crystallographic studies, in the protein the fluorophore is embedded in a hydrogen-bonded network and buried within a cylindrical 11-stranded β-barrel.[3−5] This rigid surrounding favors the high fluorescence quantum yield of ≈0.8.[6] Upon denaturation, the interior of the barrel becomes exposed, and chromophore fluorescence is rapidly quenched, comparable to the behavior of model chromophores in various organic solvents and water.[7,8] Detailed steady-state and kinetics studies of the light emission of GFP corroborate[9,10] the prominent role of excited-state proton transfer (ESPT) in the photophysics of GFP. The room-temperature absorption spectrum of wild-type GFP (wt-GFP) is characterized by two maxima, which have been attributed[9−11] to different thermodynamically stable charge states of the chromophore: the maximum at ≈398 nm to a neutral A-form; the maximum at ≈478 nm to a B-form with a deprotonated phenolic group. Decay of excited A mainly proceeds through the excited state of an intermediate I with fluorescence emission at ≈508 nm, containing the deprotonated chromophore in a nonequilibrated protein environment.[3,4,9−11]

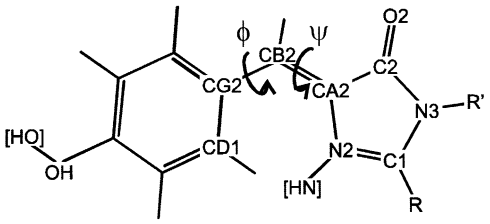

Figure 1. Structure of 4-hydroxybenzylidene-imidazolinone (abbreviated as HBI). Atom labels are according to the wt-GFP crystal structure.[3] Titratable protons are [HN] and [HO]. R and R′ in the protein are covalently linked with the C_α atoms of Ser65 and Gly67, respectively. For the model chromphore, used in the quantum chemical calculations, the C_α atoms are replaced with methyl groups. The torsional degrees of freedom around the two ring-bridging bonds are denoted as ϕ (CD1−CG2−CB2−CA2) and ψ (CG2−CG2−CA2−N2). Rotation by 180° around ϕ leaves the structure unchanged. The configuration displayed represents ϕ = 0° and ψ = 0° (cis).

* To whom correspondence should be addressed. Telephone: +49-8161-71-3557. Fax: +49-8161-71-4517. E-mail: Christina.Scharnagl@physik.blm.tu-muenchen.de.

† Physik-Department, E14 Lehrstuhl für Physik Weihenstephan, Technische Universität München.

‡ Institut für Theoretische Physik T38, Technische Universität München.

10.1021/jp036411u CCC: $27.50
Published on Web 12/05/2003

Given the range of biotechnological applications of GFP, understanding the spectral and photodynamic properties of its intrinsic fluorescence marker in relation to the underlying protonation events is of great importance. There are clearly two principal sites of pH-sensitivity of the fluorophore—the phenolic hydroxyl (OH) and the imino nitrogen of the imidazolinone ring (N2)—leading to four relevant different protonation forms: cationic, neutral, zwitterionic, and anionic chromophore. The correlation of protonation with the photophysics of GFP is still a matter of debate. A- and B-forms have been characterized crystallographically in terms of conformational changes in the vicinity of the chromophore[3−5] as well as spectroscopically using Raman studies of a model chromophore.[12] On the basis of these investigations, the A-band has been attributed to the neutral, and the B-band to the anionic chromophore. Quantum chemical calculations[13,14] for different forms of the chromophore in a vacuum and continuum solvent found best agreement with the experimental absorption in a protein environment for the protonated heterocycle N2-atom, thereby identifying A- and B-forms with cation and zwitterion, respectively. Ground-state conversion between fluorescent anion and dark zwitterion was proposed to account for the experimentally observed fast blinking.[15] Theoretical calculations[16] of the ground-state energies of a substituted chromophore resembling denatured GFP proposed a mixture of neutral and zwitterionic forms in the range from pH = 1 to 9. Photolytic proton transfer is a classic feature of phenol photophysics.[17] In synergy with the increase in basicity of the heterocyclic nitrogen center in azaphenols, phototautomerization of bifunctional compounds[18] can efficiently compete with fluorescence and internal conversion. Taking this behavior into account suggests that the zwitterion may also play a role in the photophysics of GFP. It is therefore of primary importance to characterize the fundamental protonation events in the ground and excited states of the solvated and protein-bound chromophores, respectively.

Semimacroscopic electrostatic models have been applied successfully for the calculation of the ionization free energy of titratable groups in proteins with known structure, including, for example, bacteriorhodopsin[19] and the photosynthetic reaction center.[20] The method is based on a thermodynamic cycle linking the difference between the titration behaviors of a chemical group in the protein and the group of the same kind in a model compound in solution to differences in the electrostatic environment. In a recent analysis[21] we applied the multiconformation continuum electrostatics procedure[22,23] for the calculation of the pH-dependent Boltzmann distribution of protonation states and hydroxyl group and water orientations in wt-GFP. The calculated two-step titration behavior of the chromophore agreed very well with the experimental data and provided microscopic insight into the energetics of the multiple hydrogen-bonding arrangements and the role of individual residues. However, our calculation was restricted to the phenol/phenolate equilibrium of the chromophore and, therefore, neglects the fact that an asymmetric compound with two titration sites possesses four different protonation forms connected by microscopic acid−base equilibria. To extend the theoretical calculations, free energies for the four dissociation reactions in a reference solvent have to be provided.

Experimental solution-phase acid−base dissociation constants of a model chromophore were recently published.[12] The two pK_a's are attributed to the cation/neutral (pK_a = 1.8) and neutral/anion equilibria (pK_a = 8.2), respectively. Unfortunately, this information is not sufficient to characterize all four ground-state free energy levels of the solvated chromophore. Additionally, the experimental pK_a's are macroscopic values and might be weighted combinations of the true microscopic values. Furthermore, the lack of fluorescence of the solvated neutral and anionic chromophore[7,8] prevents a discussion of the relative excited-state thermodynamics. Given these experimental limitations, theoretical estimation of the protonation equilibria is necessary to complement the experiment. Related calculations of solution-phase acidities of titratable groups revealed[16,24−32] that the most precise determination of absolute pK_a values by correlated ab initio techniques and continuum solvation models yields values accurate to within half a pK_a unit.[28−32] Alternatively, the use of linear regression relationships between experimental pK_a's and calculated condensed-phase energies for compound classes allowed pK_a predictions within comparable error bars,[24−26] even with semiempirical methods.

We carry out the analysis in five steps. In a first step, we derived an empirical equation for the protonation energies in solvent calculated with the semiempirical AM1/COSMO[33−35] methods using a representative set of test molecules for phenolic-O and heterocycle-N, respectively. In a second step, this relationship was applied to bifunctional test molecules in order to establish which error is to be awaited from the methods and reasonable for further calculations. In the third step, we calculated the free energy changes associated with the four deprotonation reactions of the solvated HBI chromophore. In contrast to the case of the test molecules, the presence of the two ring-bridging bonds of HBI requires us to take into account both dependence of the rotational barriers on the protonation state and geometric relaxation upon solvation. For the smooth torsional energy profiles of HBI,[14,15] the harmonic oscillator approximation used in standard thermochemistry will produce incorrect results for the entropy of the internal rotation modes.[36,37] Therefore, in the fourth step, the configuration integral was evaluated numerically for the coupled two-dimensional rotor profile and allowed the estimation of the protonation entropies related to these internal degrees of freedom. In the fifth step, a Förster cycle approach[17] was used to estimate pK_a shifts upon transition to the first excited singlet (S1) state.

The calculated microscopic acid−base constants for the cation/neutral and neutral/anion ground-state equilibria (2.0 and 8.3, respectively) are in excellent agreement with recent experiments[12] and confirm the phenol/phenolate equilibrium as the source for the pH-sensitivity in the physiological range. Together with the reproduction of the titration behavior of relevant bifunctional test molecules within an average error of 0.8 pK_a units, this underlines the credibility of our model. Due to the protonation-dependent torsional barriers of the two ring-bridging bonds, we find that rotational entropy adds approximately 1.5 pK_a units to dissociation free energies involving deprotonation of the phenolic oxygen of HBI. The estimates for the excited-state pK_a's indicate that excited-state deprotonation and phototautomerization are exothermic at neutral pH with a slight preference for the zwitterion over the anionic form. For an excited state with a pK_a* value of −3.5, calculated for the neutral/anionic equilibrium for a rigid planar chromophore, we estimate a rate of deprotonation in the nanosecond time regime in the diffusion-controlled limit.

2. Methods

2.1. Theory. In this section we outline the applied hybrid quantum-classical approach for calculation of microscopic equilibrium constants of the bifunctional HBI chromophore in aqueous solvent. Solvent effects on electronic structure and molecular geometry are accounted for within the quantum

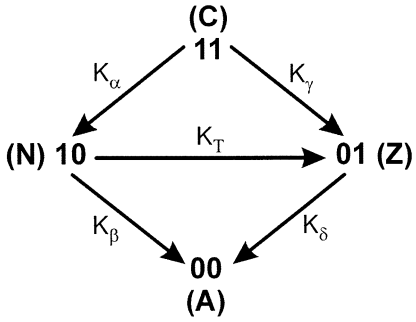

Figure 2. Protonation states and microscopic acid−base equilibrium constants for a bifunctional compound. 1 refers to a protonated site, and 0 refers to an unprotonated site. The first entry indicates the protonation state of the phenolic oxygen (OH in Figure 1), and the second entry indicates the protonation state of the imino nitrogen (N2 in Figure 1). A or 00 refers to the anion; N or 10 refers to the neutral state; C or 11 refers to the cation; Z or 01 refers to the zwitterion.

chemical scheme; conformational flexibility around internal degrees of freedom is accounted for within classical statistical thermodynamics.

2.1.1. Acid−Base Equilibria of a Nonsymmetric, Bifunctional Compound. The fluorophore of GFP (HBI, chemical structure and numbering of atoms in Figure 1) has two principal protonation sites: the phenolic oxygen (OH) and the imino nitrogen (N2). Therefore, four protonation states are available, referred to as 11 (cation, C), 10 (neutral, N), 01 (zwitterion, Z) and 00 (anion, A). The first entry indicates the protonation state of the phenolic-O; the second entry indicates the protonation state of the heterocycle-N (protonated = 1, unprotonated = 0). Figure 2 displays the definition of the four microscopic acid-dissociation constants K_α, K_β, K_γ, and K_δ connecting the four protonation states. The corresponding pK_a's (pK_α, pK_β, pK_γ, and pK_δ) are linked by a sum rule as a consequence of the state function property of the reaction free energies:

$$\mathrm{p}K_\alpha + \mathrm{p}K_\beta = \mathrm{p}K_\gamma + \mathrm{p}K_\delta \tag{1}$$

The titration behavior is characterized by two macroscopic equilibrium constants,[38]

$$K_1 = K_\alpha + K_\gamma; \quad K_2 = (K_\beta^{-1} + K_\delta^{-1})^{-1} \tag{2}$$

The tautomeric equilibrium between the two neutral states ((10, A) and (01, Z), respectively) is described by

$$K_T = \frac{[01]}{[10]} = \frac{K_\gamma}{K_\alpha} = \frac{K_\beta}{K_\delta} \tag{3}$$

The pH-dependent concentrations f of the individual protonation states follow from the pK_a's:

$$f_{11} = (1 + 10^{x_\alpha} + 10^{(x_\alpha + x_\beta)} + 10^{x_\gamma})^{-1} \tag{4a}$$

$$f_{10} = 10^{x_\alpha} f_{11} \tag{4b}$$

$$f_{01} = 10^{x_\gamma} f_{11} \tag{4c}$$

$$f_{00} = 10^{(x_\alpha + x_\beta)} f_{11} \tag{4d}$$

$$\text{with} \quad x_i = \mathrm{p}H - \mathrm{p}K_i; \quad i = \alpha, \beta, \gamma, \delta$$

2.1.2. Calculation of Microscopic Ground-State pK_a's in Solution. The microscopic equilibrium constant K for the reaction AH → A + H^+ (e.g. (α): 11 → 10 + H^+) is directly related to the standard chemical potentials of the reactants and products:

$$K = \exp(-\Delta G^\circ/RT) = 10^{-\mathrm{p}K_a}, \quad \text{with} \quad \Delta G^\circ = \mu_A^\circ + \mu_H^\circ - \mu_{AH}^\circ \tag{5}$$

ΔG° is the standard free energy of the acid dissociation, R is the gas constant (8.314 J·K^{-1}·mol^{-1}), T is the absolute temperature (298 K), and μ_A°, μ_H°, and μ_{AH}° are the standard chemical potentials of A, H^+, and AH, respectively. For a highly polarizable and conformationally flexible chromophore like HBI, the standard thermodynamical cycle[39] for decomposition of the solution free energy into the respective reaction energies in the gas phase and a term summarizing the difference between solvation energies of ionized and neutral species will fail. This pure electrostatic approach to solvation neglects energy contributions related to the deformation of the nuclear frame with solvation. It was shown[29,32] that solvated-phase relaxed structures are absolutely critical. It is, therefore, necessary to include solvation effects within the quantum chemical scheme to yield correct energy changes associated with deprotonation in aqueous solvent. Semiempirical, density functional, and ab initio techniques have previously been employed[16,24−32] to analyze molecular acidity in aqueous solution. The most precise determinations of pK_a values without fitting to experimental data yield values accurate to within half a pK_a unit.[29−32] This degree of accuracy is possible if the solute is treated at the correlated level using extended basis sets and Gaussian-*n* methods. However, scaling through linear regression for specific compound classes leads also to reliable pK_a estimation models.[24−26] These calculations revealed also[24] that bulk polarization effects as treated by continuum solvation models are far more important for yielding correct trends of the dissociation energies than solute−solvent coupling treated by microsolvation. Furthermore, it was shown that current semiempirical continuum solvation methods are not inferior to ab initio schemes. For example, reported standard deviations are below or equal to ±0.4 pK_a units for phenols and carboxylic acids obtained with semiempirical calculations,[24] ±0.24 pK_a units for carboxylic acids obtained with ab initio schemes,[26] and ±0.7 pK_a units for a series of amines obtained with density functional methods.[25] The latter investigation established also that heterocycle-N compounds carrying oxygen substituents can be included in the regression.

For a series of monofunctional reference compounds with phenolic-O or heterocycle-N, we used the semiempirical AM1/COSMO scheme[33−35] (compare section 2.2.) to calculate the protonation energy PE_{solv}°, defined as the difference in the total energy E_0 (electronic, nuclear, and solvation terms) of the protonated and unprotonated forms.

$$-\mathrm{PE}_{solv}^\circ = E_0(\mathrm{A}) - E_0(\mathrm{AH}) \tag{6a}$$

The ground-state compounds were optimized taking solvent polarization effects into account. Within the semiempirical methods used, $-\mathrm{PE}_{solv}^\circ$ is proportional (except an additional constant) to the dissociation enthalpy at room temperature.[34] Comparison with the experimental dissociation free energy ΔG_{exp}° results in an empirical relation:

$$\Delta G_{exp}^\circ = -\mathrm{PE}_{solv}^\circ + \Delta G_{cor} \tag{7}$$

where it turned out that the coefficient in the linear regression for the adopted collection of solutes is near 1. The correction term ΔG_{cor} for functional groups of a given type (O, N) includes entropy corrections to the work of deprotonation, pressure−

volume work, and μ_H°. In principle, μ_H°, the standard chemical potential of the aequeous proton can be computed from its gas-phase partition function plus the standard work of transfer from vacuum to solvent.[38,39] Experimental values for the hydration energy of the proton[39] range from −254.0 to −262.5 kcal/mol. With the room-temperature translational free energy for the proton (−7.2 kcal/mol) included, the free energy of the proton in water is between −261.2 and −269.7 kcal/mol. This energy range translates into a pK_a uncertainty of 6 units! It is, therefore, more reliable to sum up this value in the empirical correction term.

The obtained relationships were verified by prediction of microscopic pK_a's of relevant difunctional compounds with sufficient experimental characterization of all four protonation equilibria in the ground and excited states. These results were used to establish which accuracy is to be awaited from the method and which error is reasonable for further calculations.

In the development of the empirical relations (eq 7), entropy contributions due to the conformational flexibility of the ring-bridging bonds of HBI have not yet been taken into account. Recent quantum chemical calculations in vacuo[14,15] indicate rather smooth energy profiles for the internal rotation modes, depending on the protonation state of the chromophore. However, the harmonic oscillator approximation, used in standard thermochemistry,[34] produces poor and fundamentally incorrect results for the entropy of an internal rotation mode when the barrier becomes vanishingly small.[36] Therefore, we follow a hybrid quantum-classical approach proposed earlier.[38] The respective standard free energy of the acid dissociation is expressed in terms of integrals over molecular conformations

$$Z = \int \mathrm{d}\mathbf{r}\, \exp[-\beta E(\mathbf{r})] \tag{8}$$

$$\Delta G^\circ = -RT \ln \frac{\sigma_{AH}}{\sigma_A} \frac{Z_A}{Z_{AH}} + \mu_H^\circ \tag{9}$$

with $\beta = 1/RT$. $\mathbf{r} = (\phi,\psi)$ is a vector of internal coordinates specifying the conformations; $E(\mathbf{r})$ is the total energy (including nuclear, electronic, and solvation terms) for the respective protonation state as a function of the conformation; σ describes internal symmetries due to rotation around classical bonds. They have been accounted for by computing the integrals over a subset of the relevant dihedrals ($0 \le \phi \le \pi$; $0 \le \psi \le 2\pi$). Energy values $E(\mathbf{r})$ were calculated using semiempirical methods and a continuum solvation model (see section 2.2.).

To separate the effect of conformational flexibility in the configuration integrals, we introduce the energy difference relative to the minimum energy conformation $E_0(\mathbf{r}_0)$:

$$Z = \exp[-\beta E_0(\mathbf{r}_0)] \times I \tag{10a}$$

$$\text{with} \quad I = \int \mathrm{d}\mathbf{r}\, \exp[-\beta(E(\mathbf{r}) - E_0(\mathbf{r}_0))] \tag{10b}$$

The corresponding expression for the dissociation free energy (compare eq 9) becomes

$$\Delta G^\circ = -\mathrm{PE}^\circ_{solv} + \Delta G_{cor} - RT \ln\left(\frac{I_A}{I_{AH}}\right) \tag{11}$$

$-\mathrm{PE}^\circ_{solv}$ is now the energy difference calculated for the minimum energy structures of protonated and unprotonated compounds:

$$-\mathrm{PE}^\circ_{solv} = E(r_0(\mathrm{A})) - E(r_0(\mathrm{AH})) \tag{6b}$$

The additional term $-RT \ln(I_A/I_{AH})$ is related to entropy contributions associated with changes in conformational space of the ring-bridging bonds upon dissociation. The corresponding contributions to ground-state pK_a's are as follows:

$$\mathrm{p}K_a = \mathrm{p}K_a^\circ + \Delta\mathrm{p}K_a^s, \quad \text{with} \tag{12a}$$

$$\mathrm{p}K_a = \frac{\Delta G^\circ}{\ln 10 RT} \tag{12b}$$

$$\mathrm{p}K_a^\circ = \frac{(-\mathrm{PE}^\circ_{solv} + \Delta G_{cor})}{\ln 10 RT} \tag{12c}$$

$$\Delta\mathrm{p}K_a^s = -\frac{1}{\ln 10} \ln\left(\frac{I_A}{I_{AH}}\right) \tag{12d}$$

This procedure was used for each of the four microscopic equilibria with the corresponding values for ΔG_{cor}. For the other rotational degrees of freedom (e.g. the rotations of the methyl groups) we assume the same contributions to the pK_a in acid and its conjugated base.

2.1.3. Estimation of Microscopic Solution pK_a's of the Excited State. To estimate the photoinduced change in acidity, experimental pK_a shifts are related to the difference in absorption energies of A and AH using a thermodynamic cycle (Förster cylce[17]). Assuming that the excited state is sufficiently long-lived to establish the equilibria, the pK_a difference of the excited and ground states ($*$ indicates variables referring to the excited state) is

$$\mathrm{p}K_a^* - \mathrm{p}K_a = -\frac{1}{\ln 10}\left(\ln\frac{Z_A^*}{Z_{AH}^*} - \ln\frac{Z_A}{Z_{AH}}\right) = -\frac{1}{\ln 10}\left(\ln\frac{Z_A^*}{Z_A} - \ln\frac{Z_{AH}^*}{Z_{AH}}\right) \tag{13}$$

Introducing the vertical excitation energies for a given configuration $\mathbf{r}$ as $\Delta E^*(\mathbf{r})$, the energy of the excited state for this configuration is

$$E^*(\mathbf{r}) = E(\mathbf{r}) + \Delta E^*(\mathbf{r}) \tag{14}$$

This separation allows us to express the ratio of the configuration integrals for the excited and ground states for a given protonation state as the thermodynamic mean of Boltzmann factors for vertical excitation energies; the average is taken over the ground state conformational space:

$$\frac{Z^*}{Z} = \langle \exp[-\beta \Delta E^*(\mathbf{r})] \rangle_0 \tag{15}$$

The pK_a shift can be rewritten in the form

$$\mathrm{p}K_a^* - \mathrm{p}K_a = -\frac{1}{\ln 10}(\ln\langle \exp[-\beta \Delta E_A^*(\mathbf{r})]\rangle_0 - \ln\langle \exp[-\beta \Delta E_{AH}^*(\mathbf{r})]\rangle_0) \tag{16}$$

We take the excitation energies relative to the lowest energy configuration $\mathbf{r}_0$, separately for A and AH,

$$\Delta E_X^*(\mathbf{r}) = \Delta E_X^*(\mathbf{r}_0) + \Delta\Delta E_X^*(\mathbf{r}), \quad \mathrm{X} = \mathrm{A} \text{ or } \mathrm{AH} \tag{17}$$

and obtain the final expression used in the determination of the pK_a shift:

$$\mathrm{p}K_a^* - \mathrm{p}K_a = \Delta\mathrm{p}K_a^* + \Delta\Delta\mathrm{p}K_a^s \tag{18a}$$

The contributions are the difference in excitation energy for the minimum energy ground-state configurations

$$\Delta \mathrm{p}K_a^* = \frac{1}{\ln 10 RT}(\Delta E_A^*(\mathbf{r}_0(\mathrm{A})) - \Delta E_{AH}^*(\mathbf{r}_0(\mathrm{AH}))) = \frac{1}{\ln 10 RT}\Delta E_{A,AH}^* \quad (18b)$$

and the correction due to differences in the potential energy surface of the unprotonated and protonated compounds

$$\Delta\Delta \mathrm{p}K_a^s = -\frac{1}{\ln 10}\ln\left(\frac{\langle \exp[-\beta\Delta\Delta E_A^*(\mathbf{r})]\rangle_0}{\langle \exp[-\beta\Delta\Delta E_{AH}^*(\mathbf{r})]\rangle_0}\right) \quad (18c)$$

Taking vertical excitation energies and not adiabatically optimized excited-state surfaces introduces implicitly an assumption about the time scale of excited-state processes. The present results are obtained with the assumption that dissociation takes place before solvation and the geometry of the excited-state species can reach equilibrium; that is, excited-state deprotonation is the fastest deactivation channel. A recent theoretical study[40] demonstrates that the excited-state equilibrium processes in solution can increase the pK_a shift for excited phenol by 3.6 pK_a units compared to that analyzed by the Förster cycle. Analysis of the ultrafast ESPT processes in wt-GFP[41] shows that the proton-transferred configuration of the excited state is prepared directly from the equilibrium geometry of the ground-state neutral species during photoisomerization—a situation simulated in our approach (eq 16).

2.2. Computational Methods. 2.2.1. Potential Energy Surfaces. Potential energies were calculated for a model chromophore, truncated at the backbone peptide groups connecting HBI to the protein, which were replaced by CH_3 groups (compare Figure 1). To facilitate the large number of calculations necessary for the mapping of the two-dimensional conformational space spanned by the ring-bridging bonds, we use the semiempirical quantum chemical AM1 method and the COSMO[35] continuum solvation model as implemented in the MOPAC93[33−35] program package. Since the AM1 method was also used in a related study[14] for the evaluation of in vacuo energy profiles, the direct comparison between vaccum and solution-phase values is possible.

The ground-state geometries for all four protonation states were optimized at the RHF-SCF+CISD level. The CI calculations were perfomed for a six-electron/six-orbital active space. The conductor-like screening model (COSMO[35]) provides accurate gradients and allows geometry optimization of the solute within the dielectricum. The default values of the radii of the different atom types were used for the generation of the cavity. Further parameters are as follows: number of geometric segments per atomic sphere = 60, effective radius of solvent = 1.4 Å, dielectric constant = 78.4.

The potential energies (including nuclear, electronic, and solvation terms) were calculated for discrete points along the $\phi-\psi$-range (range: $-30° \le \phi, \psi \le 210°$ with step sizes $\Delta\phi$, $\Delta\psi = 30°$). At each step all other geometrical parameters were fully optimized. This adiabatic mapping assumes also that the solvent is in equilibrium with the solute at each point of the reaction path. Optimization was done until the maximal change in gradient was less than 0.01 kcal/mol; 10^{-6} au was used as the SCF convergence criterion.

Vertical excitation energies are the difference between the second and first roots of the CI matrix. A recent ab initio analysis[42] of excitations of the GFP chromophore in a vacuum including electron correlation at the MCSCF level revealed that the low-lying singlet-state excitations are solely due to $\pi \rightarrow \pi^*$ transitions and can be well described by transitions between the three highest occupied π MOs and the three lowest virtual MOs. This MO range corresponds to the choice of active space in our CISD calculation. Test calculations on the semiempirical INDO/S-SCI level were done with the program Argus.[43]

2.2.2. Evaluation of the Integrals. The potential energy surfaces are calculated by analytically fitting the 81 discrete values to a polynomial of cosine-functions in $\phi-\psi$ space:[44]

$$E(\phi,\psi) = \sum_K \sum_L A_{KL} \cos(K\phi)\cos(L\psi) \quad (19)$$

The reduction of the general Fourier series expansion of a two-rotor potential to cosine terms takes care of the symmetries $E(-\phi,\psi) = E(\phi,\psi)$ and $E(\phi,-\psi) = E(\phi,\psi)$. Imposing further the symmetry for ϕ ($E(\phi+\pi,\psi) = E(\phi,\psi)$) and ignoring higher terms leads to a reasonable fit with $K = 0$, 2, or 4 and $L = 0$, 1, 2, or 3. The inclusion of terms describing deviations from periodicity 2 for C−C rotations involving sp^2-C atoms accounts for complexities in the one-dimensional rotations, for example, minima distorted from symmetric positions. The mixed terms capture coupling of the two modes. The standard deviation for each energy value was chosen to be 0.2 eV according to the average error of AM1.[33] For numerical integration in the two-dimensional space, we used the extended trapezoid rule.[44]

3. Results

In the present study we focus on the thermodynamics of protonation events in the ground and excited states of the bifunctional GFP fluorophore in aqueous solvent. Our aim is to analyze and predict acidities and basicities direct from molecular structure calculations using quantum chemical methods and a polarized dielectric continuum representation of the solvent. We proceed in three steps: (1) generation of an empirical relation between calculated deprotonation energies and experimental dissociation free energies for monofunctional compounds, (2) test and error assessment using a representative set of bifunctional test molecules, and (3) application to HBI.

3.1. Calculation of Solution pK_a's for Test Molecules—Calibration and Error Assessment. 3.1.1. Empirical Relation for Monofunctional Compounds. The systems used for this part of the study contain either N as part of an aromatic ring (1-methylimidazole, pyridine, 8-methylquinoline) or the phenolic hydroxyl group (*p*-cresol, *p*-hydroquinone) in a rigid molecular frame. Comparable computational studies, carried out[24−26] with various levels of theory, showed that scaling through linear regression (eq 7) provides reliable pK_a prediction models.

A. Ground State. The comparison between experimental dissociation free energies and calculated solution-phase deprotonation energies is summarized in Table 1. From this comparison, the correction term (eq 7) was derived for each compound class:

$$\Delta G_{cor}(\mathrm{N}) = -209.3 \text{ kcal/mol (heterocycle-N)} \quad (20a)$$

$$\Delta G_{cor}(\mathrm{O}) = -213.9 \text{ kcal/mol (phenolic-O)} \quad (20b)$$

B. Excited State. The change in pK_a upon electronic excitation to the S1 state was estimated using the Förster cycle[17] and calculated vertical excitation energies. Generally, the change in polarity that accompanies light absorption translates into changes of proton affinity. When the N-center is part of a heterocyclic ring, the $^1(\pi - \pi^*)$-state is usually considerably

TABLE 1: Relation between Calculated Protonation Energies and Experimental Dissociation Free Energies for Model Compounds[a]

compound	pK_a	ΔG_{exp}[b]	$-PE_{solv}$[c]
	Heterocycle-N		
1-methylimidazole	6.95[d]	9.49	218.85
pyridine	5.25[d]	7.17	216.22
8-methylquinoline	4.80[e]	6.56	216.05
	Phenol-O		
p-cresol	10.17[d]	13.89	227.93
p-hydroquinone	10.35[d]	14.14	227.95

[a] All energy values are given in kcal/mol. [b] Experimental free energies are derived from the corresponding pK_a values. [c] Compare eq 6a. [d] pK_a taken from ref 58. [e] pK_a taken from ref 17.

more basic than the ground state. For 8-methylquinoline, the experimental[17] ground-state and excited-state pK_a's are 4.8 and 9.7, respectively. This upshift by 4.9 pK_a units is reproduced by the calculated difference in excitation energy $E^*(A) - E^*(AH) = 0.26$ eV, corresponding to a ΔpK_a of 4.5 units. On the other hand, phenolic compounds appear to be stronger acids in S1. The experimental pK_a values[17] for phenol are 10.0 (S0) and between 2.3 and 5.7 for S1 following the Förster cycle analysis based on emission and absorption data, respectively (the published literature value[17,40] of ≈4.0 is an average of both). The calculated difference of vertical excitation energies is −0.31 eV and corresponds to a ΔpK_a of −5.2 units. From this analysis it follows that the pK_a shift based on computed absorption data is in good accord with the experimental estimate (−4.3 pK_a units), but excited equilibrium solvation can shift the ionic dissociation thermodynamics.

3.1.2. Test and Error Assessment: Bifunctional Compounds. The empirically derived relationship between PE_{solv} and $\Delta G°$ (eqs 20a and b) was verified by prediction of microscopic pK_a's of bifunctional compounds. The fundamental requirement that the protonation events are experimentally characterized for both ground and excited states was met by hydroxypyridines (HPs)[17] with the O-function in the para- or ortho-position relative to the heterocylce-N (4- and 2-HP) and hydroxyquinolines (HQs)[17,18] with the O-function in the 7- or 8-position (7- and 8-HQ).

A. Ground State. The comparison between experimental and predicted microscopic pK_a's is summarized in Table 2. As introduced in Figure 2, the abbreviations (10) and (01) refer to the two tautomers differing in the protonation of O and N. For 2- and 4-HP it is well-known[17] that protonation of the anion takes place preferentially at the nitrogen rather than at the anionic oxygen, indicating that the hydroxypyridine form (10) is the minor fraction in water. This behavior is reproduced by the calculation. For 4-HP, the population of the keto form (01) (eq 4c) at pH = 7 is 0.5, the population of the (10)-form is 2×10^{-4}, and the tautomeric constants $K_T = [01]/[10] > 2000$. With increasing pH, the protonation state of HP compounds changes from cation to hydroxypyridine ($pK_1 \approx \min(pK_\alpha, pK_\gamma) = 2.4$) to anion ($pK_2 \approx \max(pK_\beta, pK_\delta) = 10.7$). In contrast to the case of HPs, the preferred protonation site for HQs at neutral pH is the oxygen, favoring the quinolinol (10) tautomer. The calculation predicts also the increased pK_a for O-deprotonation (pK_β) in 8-HQ as compared to 7-HQ—related to the formation of an intramolecular hydrogen bond in 8-HQ.

The absolute deviations between calculated and experimental microscopic pK_a values of the test bifunctional compounds range from 0.1 to 2.1 units with a mean of 0.8 units. The large deviation of 2.1 pK_a units, found for 8-HQ, possibly goes back to dimerization of the (01) tautomer.[18] As a result, the calculations are reliable enough to predict not only the correct sequence of protonation events but also the corresponding microscopic pK_a values with an error of ≈1 pK_a unit.

B. Excited State. A general property of azaphenols is the simultaneous increase of both the acidity of the phenolic group and the basicity of the heterocycle-N upon excitation.[17,18] Phototautomerization can be observed, in particular when each function can be anticipated to be, directly or via a bridge of hydrogen bonds, the partner of the other. This photoinduced proton transfer has been extensively characterized for HQs.[18] In the ground state at neutral pH it is the (10)-form which is favored by a factor of 2 (7-HQ, Table 2) to 28 (8-HQ) over the (01) tautomer with protonated N. In the excited state, however, it is the zwitterion that becomes favored by a very large factor, even at extreme pH values and independent of the protonation of the absorbing state. ESPT is driven by the photoinduced synergy between the two functions. For the optimized ground-state geometries, we calculate the following differences in transition energies ($\Delta E^*_{A,AH} = \Delta E^*_A - \Delta E^*_{AH}$; values in eV):

$$\text{7-HQ:}\quad \Delta E^*_{A,AH}(\alpha) = 0.19,\quad \Delta E^*_{A,AH}(\beta) = -0.54,\quad \Delta E^*_{A,AH}(\gamma) = -0.69,\quad \Delta E^*_{A,AH}(\delta) = 0.34$$

$$\text{8-HQ:}\quad \Delta E^*_{A,AH}(\alpha) = 0.18,\quad \Delta E^*_{A,AH}(\beta) = -0.41,\quad \Delta E^*_{A,AH}(\gamma) = -0.71,\quad \Delta E^*_{A,AH}(\delta) = 0.48$$

The corresponding excited-state pK_a values

$$\text{7-HQ:}\quad pK_\alpha^* = 7.7,\quad pK_\beta^* = -0.8,\quad pK_\gamma^* = -6.0,\quad pK_\delta^* = 12.9$$

$$\text{8-HQ:}\quad pK_\alpha^* = 7.6,\quad pK_\beta^* = 1.9,\quad pK_\gamma^* = -4.9,\quad pK_\delta^* = 14.4$$

lead to the macroscopic pK_a's (eq 2):

$$\text{7-HQ:}\quad pK_1^* = -6.0,\quad pK_2^* = 12.9$$

$$\text{8-HQ:}\quad pK_1^* = -4.9,\quad pK_2^* = 14.4$$

They confirm the exclusive population of the (01) tautomer in the excited state over the wide pH-range from −6 (−5) to 13 (14).

3.2. Acid−Base Equilibria of HBI in Solution. 3.2.1. Torsional Energy Profile of the Chromophore in Aqueous Solution. Due to the flexibility of the ring-bridging bonds, the geometry of HBI cannot be characterized by one dominating configuration. The inclusion of these internal degrees of freedom in a hybrid quantum-classical scheme (as outlined in section 2.1.2) requires in a first step the analysis of solvent effects on geometries and electronic structure for each of the four protonation states of the fluorophore. Table 3 summarizes the geometrical and energetic parameters resulting from the AM1/COSMO optimization. They are compared to vacuum calculations taken from the literature.[14,15] Especially the results from Voityuk el al.[14] are directly comparable to our calculations because the same level of quantum chemical theory is applied.

For the vacuum structures, the bond orders of the ring-bridging bonds (CG2−CB2, ϕ) and (CB2−CA2, ψ) can be characterized as single/double (neutral, cation), partial double/partial double (anion), and double/single (zwitterion).[14,15,45] The interaction with the polarization field of the continuum solvent induces drastic structural effects—especially for the two forms (00, 01) with deprotonated phenolic-O. Irrespective of the

TABLE 2: Comparison of Calculated and Experimental Microscopic pK_a's of Bifunctional Compounds[a]

		α (11 → 10)		β (10 → 00)		γ (11 → 01)		δ (01 → 00)				
compound		$-PE_{solv}$	pK_α	$-PE_{solv}$	pK_β	$-PE_{solv}$	pK_γ	$-PE_{solv}$	pK_δ	pK_1	pK_2	K_T
4-hydroxypyridine	calc	217.22	5.8	223.84	7.3	217.22	2.4	223.92	10.7	2.4	10.7	2512
	exp				[7.76[b]][e]		3.20[b]		11.12[b]	3.20[b]	11.12[b]	
			[6.56[c]][e]		[7.83[c]][e]		3.27[c]			3.27[c]		1950[c]
2-hydroxypyridine	calc	215.13	4.4	222.71	6.5	213.26	−0.5	224.87	11.4	−0.5	11.4	80000
	exp						0.75[b]		11.65[b]	0.75[b]	11.65[b]	
7-hydroxyquinoline	calc	215.51	4.5	225.32	8.4	221.72	5.7	219.11	7.2	4.5	8.4	0.06
	exp		5.68[b]							5.68[b]	8.90[b]	
			5.48[d]		8.85[d]		[5.78[d]][e]		[8.55[d]][e]	5.48[d]	8.85[d]	0.5[d]
8-hydroxyquinoline	calc	215.48	4.5	225.94	8.8	223.45	7.0	217.90	6.3	4.5	8.8	0.003
	exp		5.02[b]		9.81[b]					5.02[b]	9.81[b]	
			5.13[d]		9.89[d]		[6.58[d]][e]		[8.44[d]][e]	5.13[d]	9.89[d]	0.035[d]

[a] All energy values are in kcal/mol. PE_{solv} is definied in eq 6a; pK_α, pK_β, pK_γ, and pK_δ are defined in Figure 2; pK_1 and pK_2 are defined in eq 2; K_T is defined in eq 3. [b] Values from ref 58. [c] Values from ref 25. [d] Values from ref 18. [e] Experimental values in square brackets were calculated using the thermodynamic cycle (eq 1) and the given tautomeric constant K_T.

TABLE 3: Geometrical and Energy Parameters for HBI in the Gas Phase and Aqueous Solvent[a]

		bond CG2−CB2; dihedral ϕ				bond CB2−CA2; dihedral ψ					
protonation	solvent	ϕ_0	l_0/Å	$\Delta E^{\#}$	$(\Delta E^{\#})^*$	ψ_0	l_0/Å	$\Delta E^{\#}$	ΔE^{ct}	$(\Delta E^{\#})^*$	$(\Delta E^{ct})^*$
00	vacuum	0.0	1.395	22.4[b]	−18.8[b]	0.3	1.380	26.4[b]	3.6[b]	−21.2[b]	—[b]
				20.9[c]	−1.1[c]			26.2[c]	1.0[c]	−3.4[c]	1.4[c]
	water	−1.5	1.425	4.1	24.2	−0.4	1.359	19.6	4.3	2.7	0.5
01	vacuum	10.1	1.367	17.5[b]	2.8[b]	13.0	1.407	7.8[b]	—[b]	19.0[b]	—[b]
				33.9[c]	−24.4[c]			7.3[c]	1.2[c]	1.5[c]	−0.7[c]
	water	−16.2	1.416	4.3	23.5	3.8	1.365	9.7	2.1	12.2	1.1
10	vacuum	23.5	1.446	2.0[b]	30.5[b]	0.6	1.348	37.0[b]	4.7[b]	−12.9[b]	—[b]
				4.1[c]	3.9[c]			54.7[c]	−0.3[c]	−25.8[c]	−1.2[c]
	water	32.7	1.447	<0.5	10.4	2.2	1.349	29.6	4.3	−5.7	−1.1
11	vacuum	−34.8	1.437	3.6[b]	−5.1[b]	−2.9	1.355	30.0[b]	—[b]	−20.3[b]	—[b]
	water	−36.0	1.446	<0.5	19.6	−2.3	1.349	25.3	2.8	−2.7	0.0

[a] All energy values are given in kcal/mol. Equilibrium dihedrals and bond lengths of the ring-bridging bonds are referred to as ϕ_0, ψ_0, and l_0. ΔE^{ct} is the cis−trans asymmetry (rotation by 180° around ϕ leaves the structure unchanged). $\Delta E^{\#}$ denotes the rotation barrier as measured from the cis isomer (negative values indicate a 90° twisted minimum). Values with * refer to the excited state. [b] Gas-phase values from ref 14. [c] Gas-phase values from ref 15.

protonation state, the bond connecting the hydroxybenzylidene ring is a single bond, and the bond connecting the imidazolinone ring is of double-bond character. These changes can be rationalized by analysis of the mesomeric structures. For the anion, two basic resonance structures contribute to the overall wave function: the phenolate structure with the negative charge localized at the phenolic oxygen[14,15] and the enolate form with the keto-carbonyl at the benzylidene and the negative charge localized in the imidazolinone ring. For the phenolate the CG2−CB2 bond is a single bond, and the CB2−CA2 bond is a double bond; for the enolate, the bond orders are inverted.

The partial double-bond order for CG2−CB2 and CB2−CA2 of the anionic form in a vacuum indicates equal participation of enolate and phenolate mesomeric structures in the wave function.[14] Protonation of N2 in the (01)-form stabilizes the enolate, whereas protonation of OH in the (10)-form stabilizes the phenolate structure. The different bond orders for the anion and the zwitterion in solution indicate that the polarization field of water stabilizes the phenolate form in a way similiar to protonation of the phenolic-O. This is corroborated by analysis of Mulliken charges at the phenolic-O. In the anion its negative charge increases from −0.46 *e* to −0.71 *e*, and in the zwitterion it increases from −0.35 *e* to −0.68 *e*, while the response of the carbonyl-O in the imidazolinone ring (O2) is smaller than 0.1 *e*. Concomitant with the change of the charge distribution, an increase in dipole moment is registered (Table 4). The similiarity of bond orders for the zwitterion can be rationalized by the approximate balance of stabilization of the enolate form upon protonation of N2 and stabilization of the phenolate form by interaction with the reaction field. Solvent-induced structural changes in the double-bond stretching region of anionic HBI were recently revealed by Raman spectroscopy.[12] The coupling between solute and medium can additionally be quantified by the contributions to solvation energy (Table 4): interaction with the reaction field dominates, and the geometry relaxation contributes to a minor fraction. The larger dipole moment of the zwitterion provides an explanation for the increased solvation energy as compared to that of the neutral form.

TABLE 4: Total Energies, Contributions to Solvation Energies, and Dipole Changes of the HBI Chromophore[a]

protonation	E^b	$\Delta W_s{}^c$	$\Delta W_r{}^d$	$\Delta W_{solv}{}^e$	$\mu_{vac}{}^f$	$\mu_{solv}{}^g$
00	435.6	−73.7	−2.1	−75.8	9.5	20.4
01	221.3	−31.2	−2.9	−34.1	10.5	26.4
10	212.2	−18.9	−0.5	−19.4	3.6	5.2
11	0.0	−61.4	−0.5	−61.9	8.5	12.3

[a] Energy values are given in kcal/mol; dipole moments are given in Debye. [b] E: total energy of the solution-phase geometries relative to the cation. [c] ΔW_s: energy lowering for gas-phase structures due to the solvent reaction field. [d] ΔW_r: energy lowering due to geometry relaxation in solvent. [e] ΔW_{solv}: net energy lowering in aqueous solution ($\Delta W_{solv} = \Delta W_s + \Delta W_r$). [f] μ_{vac}: dipole moment of gas-phase structure. [g] μ_{solv}: dipole moment in solvent.

The torsional potential surfaces (PESs) for the four protonation states are displayed in Figures 3 and 4. The curves are the result of the fitting procedure outlined in section 2.2.2. Standard deviations for all 81 points used in the fitting procedure are 0.12 eV (00), 0.04 eV (01), 0.13 eV (10), and 0.13 eV (11) for the ground state and 0.10 eV (00), 0.11 eV (01), 0.11 eV (10), and 0.10 eV (11) for the excited state. The error bars are, therefore, in the range of the systematic error of the method

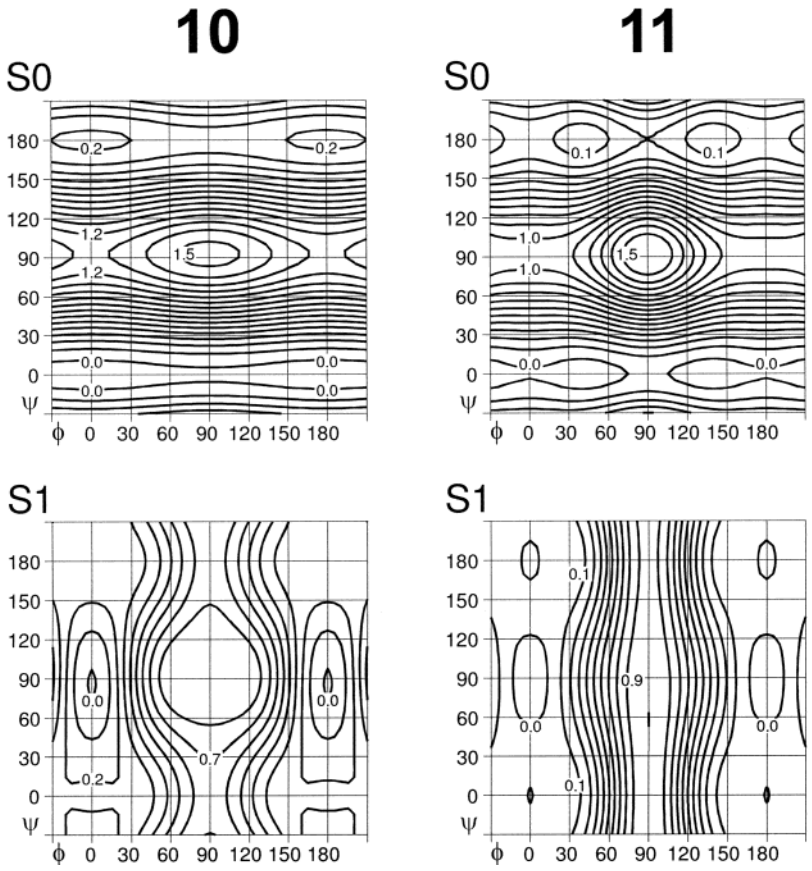

Figure 3. Energy profiles for coupled rotation around the ring-bridging bonds in the ground (S0) and excited (S1) states. The curves are the result of analytically fitting discrete values, calculated for a step size of 30° in each direction, to the coupled-rotor potential of eq 19. The values are relative to the respective minimum energies (Table 3). The spacing between equipotential lines is 0.1 eV (2.4 kcal/mol). For the definition of the dihedrals see Figure 1. 10 refers to the neutral state, and 11 refers to the cation.

(0.2 eV, compare with section 2.2.1). The energy profiles for the ground states show a close correspondence to the bond orders discussed above. The CG2−CB2 bond (dihedral ϕ) for neutral and cationic forms is generally characterized by a very flat torsional profile.

Potential energies for the S1 state are reconstructed from vertical transition energies and, therefore, do not represent adiabatic surfaces (compare with section 2.1). The semiempirical AM1 method is in principle inferior for calculations of excited-state properties as compared to programs such as INDO/S[43] or OM2,[15] which are parametrized for excited-state calculations. However, it was reported[14] that the application of AM1 at the CISD level of theory results in excitation energies for conjugated systems that agreed reasonable well with experimental data and high-level ab initio calculations. Furthermore, it was argued that even these high-level theories are not accurate enough to reproduce absolute excited-state energies.[46] In the present analysis we use energy differences which are more reliably predicted, by both semiempirical and ab initio schemes. To test the quality of the calculations further, we compared calculated transition energies for the solution-phase structures with experimental absorption spectra (Table 5). This comparison proves the close correspondence between calculated and experimental energy differences as well as the reproduction of the correct variation of the absorption energies with the protonation state. In detail, we calculate $\Delta\lambda_{abs}(00-10) = -66$ nm (exp: $-57/-60$ nm), $\Delta\lambda_{abs}(00-11) = -41$ nm (exp: $-35/-42$ nm), and $\Delta\lambda_{abs}(10-11) = 25$ nm (exp: 15/18 nm). No experimental values for the zwitterion are available. Besides the energy differences, the shifts in absorption wavelength with increased polarity of the solvent are in correspondence with reported experimental values.[7,12,47] In a polar solvent, the anion absorbs red-shifted[7] and changes its structure, as revealed by changes of the Raman spectrum in the double-bond stretching region.[12] In contrast to the case of the anion, the absorption maximum of the neutral form is independent of the solvent,[7] and only a slight variation upon increased polarity is calculated and measured (range: 373−386 nm[7]) for the cation.

The comparison with the calculated vacuum values[14] shows how the interaction with the solvent polarization field changes the vertical excited-state torsional profiles of the central bonds (Table 3). In line with the established single-bond character of the CG2−CB2 bond in the ground state, a large barrier in the S1 state stabilizes the planar geometry, irrespective of the protonation state of the fluorophore. The energy profiles for rotation around the CB2−CA2 bond indicate that protonation of the phenolic-O stabilizes an orthogonally twisted geometry in the S1 state for neutral and cationic forms. For the zwitterion and the anion, we note also a destabilization of the planar geometry relative to the ground state but no stabilization of a twisted geometry. Generally, the profiles are very flat. It has to be emphasized that the excited-state torsional profiles are not adiabatic surfaces; excited-state relaxation of the chromophore geometry and the solvent surroundings will modify the gradients of the curves.

The changes of the energy profiles can be rationalized regarding the differences in bonding/antibonding character of frontier π-orbitals in the region of the central methine bridge under the influence of the continuum solvent model. Of special interest here is the anion. The polarization field stabilizes the

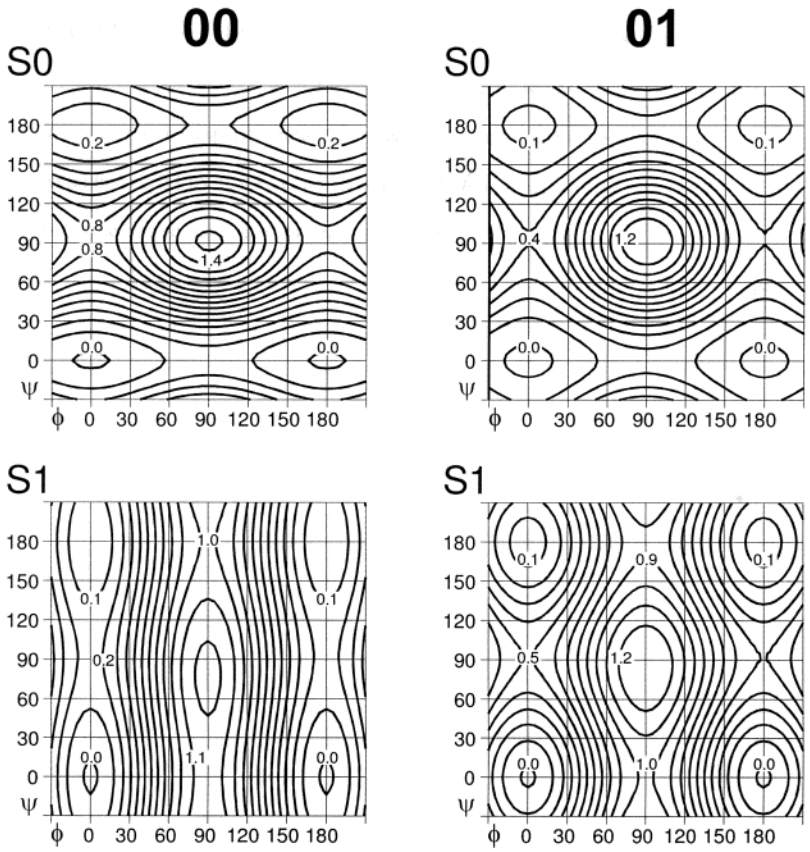

Figure 4. As in Figure 3: 00 refers to the anion, and 01 refers to the zwitterion.

TABLE 5: Comparison of Calculated and Experimental Absorption Wavelengths λ_{abs} of the HBI Chromophore in Different Protonation States

	λ_{abs}/nm for structure[a]/solvent[b]			
	vacuum/vacuum	vacuum/water	water/water	experiment/water
00	443 464[c] 479[d]	418	389	428,[e] 425,[f] 426[g]
10	326 336[c] 340[d]	325	323	368,[e] 368,[f] 370[g]
11	413 403[c]	355	348	393,[e] 386,[f] 396[g]

[a] Chromophore structure after optimization in a vacuum or water, represented by a continuum model. [b] The solvent for the calculation was either vacuum or a dielectric continuum. [c] Result of INDO/S-SCI calculation. [d] Value from ref 15. [e] Value from ref 12. [f] Value from ref 7. [g] Value from ref 47.

phenolate mesomeric structure in the ground state, thereby strengthening the antibonding character of the CG2−CB2 bond and the bonding character of the CB2−CA2 bond in the highest occupied orbital (HOMO). Excitation under the influence of the solvent polarization field concentrates electronic density at the central atom of the bridge (CB2) and produces a lowest unoccupied orbital (LUMO) which is neither bonding nor antibonding with respect to CG2 and CA2. The HOMO−LUMO transition reduces therefore the bonding $\pi-\pi$ interaction character of the CB2−CA2 bond, resulting in a relative destabilization of the planar geometry.

3.2.2. Microscopic Acid−Base Equilibria of HBI in the Ground State. For the solvated GFP chromophore, two points have to be addressed: (1) as shown by the very flat PES, several conformations of the central methine bridge can be populated, and (2) the conformational flexibility in this region changes with the protonation state (Figure 3). In the first step we calculated protonation energies between the optimized geometries for the four microscopic acid−base transitions and translated these values with the help of the empirical relationship (eqs 7 and 20) into dissociation free energies. In the second step, changes in the PESs of protonated and unprotonated compounds are taken into account. This required the evaluation of the relative configuration integrals I (eqs 10 and 11) over the two-dimensional coupled-rotor energy profiles. The corresponding values (in units of $(2\pi)^m$; $m = 2$ = number of internal degrees of freedom) are $I_{00} = 0.011$, $I_{01} = 0.014$, $I_{10} = 0.271$, and $I_{11} = 0.234$. To estimate the error of this procedure, we apply the standard deviation for energy values (0.2 eV) and assume that 25% of the points in the integration region are populated with a Boltzmann factor of 1, while the rest is not populated. Applying error propagation results in an upper limit for the standard deviation for the integral of $\sigma_I = 0.008$. The contributions to the pK_a values according to eq 18 are summarized in Table 6A. The difference in conformational flexibility as reflected by the configuration integrals has large effects on equilibria involving a change of the protonation state of phenolic-O (pK_β,pK_γ). A ratio I_A/I_{AH} of approximately 0.01/0.25 corresponds to a pK_a upshift of 1.3 units. The direction of the shift is in accord with the reduction of the rotational space upon deprotonation, leading to negative dissociation entropy.[37]

The two transitions in the pH-titration of HBI correspond to the cation/neutral equilibrium in the acidic pH-region (pK_α = 2.0) and the neutral/anion equilibrium (pK_β = 8.3). These values calculated for the flexible chromophore are in excellent agreement with experimental pK_a's published recently (1.8 and 8.1).[12] The comparison to the values for a rigidly planar fluorophore (pK_α = 1.5, pK_β = 6.6) emphasizes the role of the internal rotational degrees of freedom for adjusting the pK_a.

TABLE 6: Energy and Entropy Contributions to the Microscopic Acid−Base Equilibria of HBI in Aqueous Solvent

(A) Ground State

rigid[a]	α(11→10)	β(10→00)	γ(11→01)	δ(01→00)	pK_1	pK_2	K_T
PE°_{solv} [c,d]	211.32	222.97	220.08	214.20			
pK_a [e]	1.5	6.6	4.5	3.6	1.5	6.6	10^{-3}
flexible	α(11→10)	β(10→00)	γ(11→01)	δ(01→00)	pK_1	pK_2	K_T
PE°_{solv} [b,c,f]	212.19	223.38	221.26	214.32			
pK°_a [e]	2.1	6.9	5.4	3.6			
ΔpK^{s}_a [g]	−0.1	+1.4	+1.2	+0.1			
pK_a [h]	2.0	8.3	6.6	3.7	2.0	8.3	2×10^{-5}

(B) Excited State

rigid[a]	α(11→10)	β(10→00)	γ(11→01)	δ(01→00)	pK_1	pK_2	K_T
$\Delta E^*_{A,AH}$ [c,i]	+6.60	−13.79	−13.46	+6.25			
ΔpK^*_a [i]	+4.8	−10.1	−9.9	+4.6			
pK^*_a [j]	6.3	−3.5	−5.4	8.2	−5.4	8.2	5×10^{11}
flexible	α(11→10)	β(10→00)	γ(11→01)	δ(01→00)	pK_1	pK_2	K_T
$\Delta E^*_{A,AH}$ [b,c,i]	+6.50	−15.15	−16.07	+7.42			
ΔpK^*_a [i]	+4.8	−11.1	−11.8	+5.6			
$\Delta\Delta pK^{s}_a$ [k]	+0.2	+2.9	+3.4	−0.3			
pK^*_a [j]	7.0	0.1	−1.8	8.9	−1.8	8.9	6×10^{8}

[a] ($\phi = 0, \psi = 0$). [b] ($\phi = \phi_0, \psi = \psi_0$); compare Table 3. [c] Energy values in kcal/mol. [d] Eq 6a. [e] Eqs 12c and 20. [f] Eq 6b. [g] Eq 12d. [h] Eq 12a. [i] Eq 18b. [j] Eq 18a. [k] Eq 18c.

3.2.3. Estimation of Protonation Equilibria in the Excited State. The pK_a shifts upon excitation are calculated from the differences in vertical transition energies of protonated and unprotonated species using a thermodynamic approach similiar to the Förster cycle (as outlined in section 2.1.3). With the calculated excitation energies (Table 6B) we find that pK_β and pK_γ undergo a significant downshift of approximately 11 pK units while pK_α and pK_δ are shifted up by 5 units. To these shifts add corrections due to differences of the PES (eq 18c) in the form of the average of Boltzmann factors for relative excitation energies $\Delta\Delta E^*$ taken over a ground-state ensemble. The values for $\ln\langle\exp(-\beta\Delta\Delta E^*)\rangle_0$ calculated for the individual protonation states are 0.83 (00), 0.09 (01), 7.42 (10), and 7.85 (11). The corresponding pK_a corrections ($\Delta\Delta pK^s_a$ in Table 6B, eq 18c) affect again those equilibria involving a protonation change of phenolic-O and lead to an upshift of pK_β and pK_γ by approximately 3 units. The final values, summarized in Table 6B, show that the predicted protonation events in the excited state correspond now to the cation/zwitterion transition (pK_γ = −1.8) and zwitterion/anion equilibrium (pK_δ = 8.9). The reliability of the values can be examined using the experimental absorption energies (Table 5) in the Förster cycle. The corresponding pK_a shifts upon excitation are $\Delta pK^*_\alpha = +3.6$ (calc: +5.0) and $\Delta pK^*_\beta = -8.0$ (calc: −8.2). The comparison between theoretical and experimental estimates confirms again the error of approximately 1 pK unit. The value of $pK^*_\beta = 0.1$ for dissociation of the excited neutral chromophore is comparable to those of other aromatic hydroxyl compounds, for example, naphthol ($pK^*_\alpha = 0.5$[43]) or merocyanine ($pK^*_\alpha = 1.9$[44]). The sum rule (eq 1) gives also a range for the sum of changes for the accompanying microscopic equilibrium: $\Delta pK^*_\gamma + \Delta pK^*_\delta = -4.4$ (calc: −3.2).

The predicted behavior for the excited state of HBI resembles the behavior of azaphenols (e.g. HP, HQ; discussed in section 3.2). Assuming that the S1 state is sufficiently long-lived to establish the protolytic equilibria, the synergy effect between increased acidity of the phenolic-O and increased basicity of the imino-N favors the zwitterionic state over a wide pH-range. Whether the protolytic equilibrium can be reached depends on the availability of a fast pathway for the proton competing with other decay channels, for example, internal conversion.

4. Discussion

Given the range of biotechnological applications of GFP, characterization of the protonation states of its intrinsic fluorescence marker in the ground and excited states is of great importance. However, the nature of protonation events and their connection to the photophysics are still subjects of debate. Spectroscopic[12,50] and structural analysis[3−5] provide strong arguments for a ground-state equilibrium between neutral and anionic forms. Photoinduced increase of the acidity of the phenolic hydroxyl of HBI provides the driving force for excited-state deprotonation.[9,10] On the basis of quantum chemical calculations[14−16] it was argued that zwitterionic and/or cationic forms of the chromophore may also be involved. Ground-state conversion between fluorescent anion and dark zwitterion was proposed[15] to account for the experimentally observed fast blinking. However, no experimental evidence has yet been found for the existence of the zwitterion.[12,50] Experimental characterization of the ground-state equilibria by pH-titration[12] of a model chromophore attributes the two pK_a's to the cation/neutral (pK_a = 1.8) and neutral/anion (pK_a = 8.2) transitions, respectively. However, the measured values are macroscopic values and obscure the fact that the bifunctional compound possesses four microscopic acid−base equilibrium constants.

Due to these experimental limitations, theoretical calculations are a true alternative. It is the aim of our present study to quantify the thermodynamic stability of each of the four protonation states in aqueous solvent in the ground and excited states. In addition, the solution-phase pK_a's are necessary reference inputs for the calculation of the corresponding free energy levels in the protein by means of multiconformational continuum electrostatic methods.[20−23] Reduction of the analysis to one selected equilibrium (as done in our previous contribution[21] for the neutral/anion transition) may be misleading. pK_a shifts due to electrostatic interactions and desolvation in the protein interior

can be as large as 9 pK_a units, as in the case of rhodopsin.[51] Equilibria being outside the physiologic range in solvent can therefore be brought into the functionally relevant pH-region upon binding of the chromophore to the protein.

4.1. Reliability and Limits of Methods. With the aid of a thermodynamic cycle, conventional methods[16,24−32,39,40] relate the pK_a of an acid to its gas-phase acidity and the free energies of solvation of the neutral and ionic species. Quantum chemical methods (ab initio, density functional, or semiempirical) are used to determine geometries and energies in the gas phase, while the solvation free energies are obtained, for example, with polarizable continuum solvation models[24−32] or mixed quantum mechanical/molecular mechanical methods.[40] While this standard procedure is justified for rigid molecules such as phenol, imidazole, or carboxylate, it turned out that it fails for the HBI chromophore due to the presence of soft internal degrees of freedom. This has two reasons: First, the use of solution-phase geometry optimization[29,32] proved important to take care of solvent-induced conformational changes (contributions: $\Delta E_{max} = 3$ kcal/mol. Table 4). Second, an extended thermodynamic scheme[37] has to account for entropy contributions to the dissociation free energies due to distinct conformational flexibility of the two ring-bridging bonds mediated by the protonation state. The presence of vanishingly small rotational barriers for ionization states with protonated phenolic hydroxyl implies that the harmonic oscillator approximation used in standard thermochemistry[34] will produce incorrect results for the entropy of the internal rotation modes.[36,37] In addition, the conjugated π-system requires us to take the coupling of the two internal modes into account. The applied hybrid quantum-classical scheme reproduces pK_a's for ground-state equilibria in good agreement with experiment (see section 3.1). The evaluation of the configuration integrals (eqs 12 and 18) requires—for all four protonation states—geometry optimization in solution phase for a large number of discrete points in configuration space. Due to these great demands to computational power, we employed here the semiempirical AM1/COSMO level of theory. However, the methods outlined in section 2.1. are applicable with more accurate quantum chemical models to avoid the deficiencies of semiempirical methods,for example, the overestimation of barriers for rotation around double bonds.[52] Nevertheless, as was shown in eqs 12 and 18, the calculations of pK_a's can be reduced to the evaluation of relative energy differences, which are reliably reproduced by the semiempirical methods (compare e.g. Table 5), too.

For the estimation of excited-state equilibrium constants, there is a great deal of uncertainty in the relaxation processes of the solvated excited-state species and the related time scales. First of all, one has to assume that the lifetime of the excited state is sufficiently long to establish the protolytic equilibria. In that case, the primary photoreaction is determined by the interplay between internal vibrational or conformational relaxation, solvent reorganization, and proton transfer, which can provide either dominating or competing pathways.[49] Accordingly, there are different procedures to handle the excited equilibrium processes in solution. The assumption that the excited-state acid and the surrounding solvent can reach equilibrium before ionic dissociation takes place and that the conjugated base is produced in the first excited state requires the calculation of adiabatic excited-state potential energy surfaces under equilibrium solvation conditions—similiar to the procedure outlined for the calculation of ground-state equilibria. On the other hand, if ESPT is the fastest relaxation process, chromophore geometry and solvent correspond to the ground-state arrangement and the vertical transition energies are the relevant energies to relate excited-state pK_a's to the ground-state values. Excited-state pK_a's calculated for phenol with both procedures[40] differ by ≈3 pK_a units; full solvent equilibration further stabilizes the excited phenolate ion. In the general case, nonequilibrium effects will be encountered. Analysis of the ultrafast optical response of wild-type GFP[41] indicates that ESPT is the fastest decay channel in the protein. The proton-transferred configuration is prepared directly from the equilibrium geometry of the ground state of the neutral species during photoexcitation. The procedure used in the present calculation of excited-state acidities simulates this situation. The stop of ESPT with full equilibration of the excited protonated species[41] hints to a shift in proton affinity after vibrational relaxation and internal conversion. However, the order in which the nonradiative decay pathways are activated may differ for protein-bound and solvated chromophore.

4.2. Contributions to Ground-State Equilibria. On the basis of characteristic absorption spectra of cationic, neutral, and anionic forms of a model chromophore in aqueous solvent, the macroscopic pK_a values have recently been attributed[12] to imidazolinone ring nitrogen (1.8) and phenolic hydroxyl (8.2) deprotonation. The pK_a for the neutral/anion equilibrium is also very close to the value of 8.1 reported for the denatured wild-type protein.[53] The results of our calculations (p$K_\alpha = 2.0$ and p$K_\beta = 8.3$, respectively; see Table 6A) are in excellent agreement with these experimental findings. Together with the reproduction of the titration behavior of relevant bifunctional test molecules (within an average error below 1 pK_a unit; compare Table 2), this underlines the credibility to our model. Besides these two pK_a's (Table 6A), we obtain the microscopic constants for the neutral/zwitterion equilibrium (p$K_\gamma = 6.6$) and the zwitterion/anion equilibrium (p$K_\delta = 3.7$), which are not available from experiment. The tautomeric constant ($K_T = 2 \times 10^{-5}$) confirms that the zwitterionic form will not be populated in the ground state.

In addition to the evaluation of the free energy differences of the four protonation states, we are able to dissect the constituents that govern the microscopic equilibria in solution. Besides enthalpic contributions, the configurational space of internal degrees of freedom changes when going from the phenolic acid to the conjugate base. The corresponding reaction entropy adds up to 1.5 pK_a units to the equilibrium constants involving deprotonation of the phenolic hydroxyl. Whereas the pK_a for the neutral/anion equilibrium (pK_β) calculated for a rigidly planar chromophore is 6.6, the evaluation of the configuration integral over the whole space of conformational flexibility of the two ring-bridging bonds brings this value in accord with the experiment (8.3). If we assume a transition from free rotation to harmonic oscillation if going from the phenol to the phenolate form and apply Pitzer's tables,[36,37,54] we calculate an entropy correction of 1.2 pK_a units, in close agreement with the evaluation of the configuration integrals in our extended treatment. The selective restriction of motion along these internal degrees of freedom upon binding of HBI to the apoprotein in GFP is therefore a dominant contribution to the adjustment of microscopic pK_a's in protein, as discussed in our previous contribution.[37]

4.3. Excited-State: Deprotonation or Tautomerization Competing with Isomerization? The nature and the order of the processes that follow photoexcitation of the HBI chromophore in GFP and solvent are still open questions. Possible competing decay pathways involve fluorescence, ESPT to solvent or protein, inter- and intramolecular vibrational energy transfer, and internal skeletal dynamics coupled to internal

conversion via torsional motion of the chromophore. The activation of individual channels depends on the surrounding matrix, thereby emphasizing the fact that the photoexcited system proceeds along a multidimensional reaction path including both internal solute coordinates (e.g. nuclear dynamics, intrinsic basicities and acidities) and external solvent coordinates (e.g. hydrogen-bond reorganization, dipole relaxation).

The contribution of the surrounding matrix to the dynamical complexity shows up in the comparison of excited-state processes in the protein and in solvent. In GFP, the chromophore is embedded in an extended hydrogen-bonded network. Excited-state deprotonation occurs within 3 ps[9,10] and is the fastest decay channel.[41] The transferred proton binds to internal water molecules or protein residues. The photoproduct shows high fluorescence quantum yield even at ambient temperature. Those properties that distinguish the GFP protein cannot be observed for the free chromophore. In most of the solvents it exhibits only weak fluorescence at room temperature.[7] However, the quantum yield increases to values comparable to those of the protein upon cooling below the glass transition temperature of the solvent matrix[7,55] or in high viscosity solvents.[8] These observations were attributed to the inhibition of rapid internal conversion involving motion with considerable amplitude. It was established[55] that the free chromophore in low-temperature alcoholic solution shows a spectral and photochemical reaction pattern similiar to that of the chromophore embedded in the protein matrix. In a poly(vinyl alcohol) (PVA) matrix, even ESPT is recoverd (P. Schellenberg, private communication).

Our analysis adds a new possibility for an ESPT process: phototautomerization leading from neutral to zwitterionic forms, driven by the synergy between increased acidity of the phenolic hydroxyl and increased basicity of the heterocycle-N function. The free energy differences (Table 6B) show that the formation of the zwitterion in the excited state is exothermic for pH values up to 9. However, a prerequisite for efficient proton transfer is the availability of a hydrogen-bonded complex of hydroxylic solvent molecules being able to shuttle protons back and forth between the two functions. Possible transport modes are (i) fast multiple ESPT proceeding via a preformatted cyclic bridge of solvent molecules and (ii) stepwise transport involving excited anion or cation as competitive intermediates and solvent molecules as proton exchange partners. For a related bifunctional molecule, 7-hydroxyquinoline, time constants lower than 10 ps have been reported for phototautomerization[18] proceeding via mode (i) involving two linking solvent molecules.

A discussion of the dynamical behavior of the excited species requires estimates for the time scales of the involved processes. An estimate for the average lifetime of the neutral GFP chromophore in the absence of excited-state deprotonation and isomerization is 200 ps[8] (deexcitation rate constant $k_N^* \approx 10^9$ to 10^{10} s^{-1}). Estimates for excited-state conformational relaxation processes are available, for example, for the protonated Schiff base in bacteriorhodopsin or protonated merocyanine dyes.[49,56] There, fast photoinduced skeletal dynamics in the sub-picosecond regime is coupled to slower angular modes in the range of several picoseconds. The pK_a value for deprotonation of the phenolic hydroxyl calculated for the excited state of the neutral, rigidly planar chromophore without reorganization of solute and solvent (YH_p^*) is -3.5 (pK_β^* in Table 6B), leading to an equilibrium constant for the dissociation reaction

$$YH_p^* + H_2O \underset{k_a}{\overset{k_d}{\leftrightarrow}} Y_p^-{}^* + H_3O^+$$

of $K_\beta = k_d/k_a = 10^{3.5}$. If protolytic equilibrium is assumed, the deprotonation rate constant is $k_d = k_a K_\beta$. If we further assume that reprotonation is a diffusion-controlled process with a H^+-diffusion constant of $k_D = 10^{10}$ M^{-1} s^{-1} at ambient temperature,[48,49] the deprotonation rate at pH 6 is $k_d = k_D[H_3O^+]K_\beta \approx 10^8$ s^{-1}. However, investigations of ESPT reactions show that solvent reorganization is necessary prior to successful transfer of the proton.[48,49] Assuming that solvent reorganization in the excited state affects the protonation equilibria in a way comparable to the behavior reported for phenol,[40] the stabilization of the excited phenolate anion could reduce the corresponding pK_β^* by 3 units. The corresponding time scales include, however, additional waiting times on the order of several picoseconds for dipolar reorientation. We conclude that in the diffusion-controlled limit the deprotonation time for the excited phenol-OH is in the order of several nanoseconds and, therefore, not in concurrence with internal skeletal conformational relaxation or radiative deexcitation. Formation of an excited-state cationic intermediate will be even slower (limited by the corresponding association rate constant estimated in the diffusion-controlled regime to be $k_a = 10^4$ s^{-1} (pH 6)).

Phototautomerization remains only a possibility if fast multiple correlated proton transfer takes place within a preformed hydrogen-bonded network involving at least four hydroxylic solvent molecules—a situation found, for example, in a PVA matrix or wt-GFP. There, it may be important in the blinking and photobleaching behavior of GFP, detected by single molecule spectroscopy. We like to emphasize that our estimates for the excited-state deprotonation reaction rates do not include conformational relaxation. The stop of ESPT with full equilibration of the excited neutral chromophore in GFP[41] hints to affinity changes of donor and/or acceptor coupled to relaxation dynamics. On the other hand, it was proposed[57] that internal skeletal dynamics of the isolated chromophore promotes ESPT.

5. Conclusion

We investigated the thermodynamic stability of the four protonation states of the HBI chromophore in aqueous solvent at room temperature. The use of a hybrid quantum-classical method and evaluation of configuration integrals revealed entropy contributions to the acid−base equilibria due to the protonation-dependent conformational space of the ring-bridging bonds. Calculated ground-state pK_a's are in excellent agreement with experiment and confirm the assignment of pK_a = 2.0 to the cation/neutral transition and pK_a = 8.3 to the neutral/anion transition. Together with the results from our previous studies,[21,37] we conclude that, besides electrostatic interactions, pK_a shifts associated with entropy contributions due to selective restriction of internal rotational degrees of freedom are vital determinants to ensure functionality of chromophoric groups in proteins such as GFP, bacteriorhodopsin, photosynthetic bile pigments, or sensory pigments.

The calculations of excited-state pK_a's are based on an experimental model for ESPT in GFP which indicates that the proton transferred configuration of the excited fluorophore is formed directly from an equilibrium geometry distribution of the ground-state species. The calculated excited-state free energy levels propose that synergy effects between increased acidity of the phenol-O and increased basicity of the imino-N favor the zwitterionic state over the anionic and neutral protonation states. In the diffusion-controlled limit, we estimate an excited-state deprotonation time in the nanosecond regime, which is, therefore, longer than the proposed time scales for fluorescence or internal conformational dynamics leading to internal conversion. However, the formation of low-barrier hydrogen-bond

networks and the occurrence of dipolar fluctuations in the surroundings might promote fast proton transfer. On the basis of the microscopic dissociation constants calculated in this contribution, the discussion of these energetic and kinetic aspects of the proton transfer in GFP will be the subject of further investigations.

Acknowledgment. We thank Prof. Sighart F. Fischer for encouragement and useful discussions. This work was supported by the DFG, SFB 533/TP C2, and by the Fond der Chemischen Industrie.

References and Notes

(1) Tsien, R. Y. *Annu. Rev. Biochem.* **1998**, *67*, 509.
(2) Cubitt, A. B.; Wollenweber, L. A.; Heim, R. *Methods Cell Biol.* **1999**, *58*, 19.
(3) Brejc, K.; Sixma, R. K.; Kitts, P. A.; Kain, S. R.; Tsien, R. Y.; Ormö, M.; Remington, S. J. *Proc. Natl. Acad. Sci. U.S.A.* **1997**, *94*, 2306.
(4) Palm, G. J.; Zdanov, A.; Gaitanaris, G. A.; Stauber, R.; Pavlakis, G. N.; Wlodawer, A. *Nature Struct. Biol.* **1997**, *4*, 361.
(5) Elsliger, M.-A.; Wachter, R. M.; Hanson, G. T.; Kallio, K.; Remington, S. J. *Biochemistry* **1999**, *38*, 5296.
(6) Morise, H.; Shimomura, O.; Johnson, F. H.; Winant, J. *Biochemistry* **1974**, *13*, 2656.
(7) Niwa, H.; Inouye, S.; Hirano, T.; Matsuno, T.; Kojima, S.; Kubota, M.; Ohashi, M.; Tsuji, F. I. *Proc. Natl. Acad. Sci. U.S.A.* **1996**, *93*, 13617.
(8) Kummer, A. D.; Kompa, C.; Niwa, J.; Hirano, T.; Kojima, S.; Michel-Beyerle, M. E. *J. Phys. Chem. B* **2002**, *106*, 7554.
(9) Chattoraj, M.; King, B. A.; Bublitz, G. U.; Boxer, S. G. *Proc. Natl. Acad. Sci. U.S.A.* **1996**, *93*, 8362.
(10) Lossau, H.; Kummer, A.; Heinecke, R.; Pöllinger-Dammer, F.; Kompa, C.; Bieser, G.; Jonsson, T.; Silva, C. M.; Yang, M. M.; Youvan, D. C.; Michel-Beyerle, M. E. *Chem. Phys.* **1996**, *213*, 1.
(11) Creemers, T. M. H.; Lock, A. J.; Subramaniam, V.; Jovin, T. M.; Völker, S. *Nature Struct. Biol.* **1999**, *6*, 557.
(12) Bell, A. F.; He, X.; Wachter, R. M.; Tonge, P. J. *Biochemistry* **2000**, *39*, 4423.
(13) Voityuk, A. A.; Michel-Beyerle, M. E.; Rösch, N. *Chem. Phys.* **1998**, *231*, 13.
(14) Voityuk, A. A.; Michel-Beyerle, M. E.; Rösch, N. *Chem. Phys. Lett.* **1998**, *296*, 269.
(15) Weber, W.; Helms, V.; McCammon, J. A.; Langhoff, P. W. *Proc. Natl. Acad. Sci. U.S.A.* **1999**, *96*, 6177.
(16) El Yazal, J.; Prendergast, F. G.; Shaw, D. E.; Pang, Y.-P. *J. Am. Chem. Soc.* **2000**, *122*, 11411.
(17) Stewart, R. In *The Proton: Application to Organic Chemistry*; Wassermann, H. H., Ed.; Vol. 46 of Organic Chemistry, A series of Monographs; Academic Press: New York, 1985.
(18) Bardez, E. *Isr. J. Chem.* **1999**, *39*, 319.
(19) Scharnagl, C.; Hettenkofer, J.; Fischer, S. F. *J. Phys. Chem.* **1995**, *99*, 7787.
(20) Alexov, E. G.; Gunner, M. R. *Biochemistry* **1999**, *38*, 8253.
(21) Scharnagl, C.; Raupp-Kossmann, R.; Fischer, S. F. *Biophys. J.* **1999**, *77*, 1839.
(22) Alexov, E. G.; Gunner, M. R. *Biophys. J.* **1997**, *72*, 2075.
(23) Spassov, V. Z.; Bashford, D. *J. Comput. Chem.* **1999**, *20*, 1091.
(24) Schüürmann, G. *Quant. Struct.-Act. Relat.* **1996**, *15*, 121.
(25) Kallies, B.; Mitzner, R. *J. Phys. Chem. B* **1997**, *101*, 2959.
(26) Schüürmann, G.; Cossi, M.; Barone, V.; Tomasi, J. *J. Phys. Chem. A* **1998**, *102*, 6706.
(27) Chipman, D. M. *J. Phys. Chem. A* **2002**, *106*, 7413.
(28) Topol, I. A.; Tawa, G. J.; Burt, S. K.; Rashin, A. A. *J. Phys. Chem. A* **1997**, *101*, 10075.
(29) Da Silva, C. O.; da Silva, E. C.; Nascimento, M. A. C. *J. Phys. Chem. A* **1999**, *103*, 11194.
(30) Da Silva, C. O.; da Silva, E. C.; Nascimento, M. A. C. *J. Phys. Chem. A* **2000**, *104*, 2402.
(31) Liptak, M. D.; Shields, G. C. *J. Am. Chem. Soc.* **2001**, *123*, 7314.
(32) Liptak, M. D.; Gross, K. C.; Seybold, P. G.; Feldgus, S.; Shields, G. C. *J. Am. Chem. Soc.* **2002**, *124*, 6421.
(33) Stewart, J. J. P. *J. Comput.-Aided Mol. Des.* **1990**, *4*, 1.
(34) Stewart, J. J. P. *MOPAC 93 Manual*; Fujitsu Ltd.: Tokyo, 1993.
(35) Klamt, A.; Schüürmann, G. *J. Chem. Soc., Perkin Trans. 2* **1993**, 799.
(36) East, A. L. L. *J. Chem. Phys.* **1997**, *106*, 6655.
(37) Raupp-Kossmann, R. A.; Scharnagl, C. *Chem. Phys. Lett.* **2001**, *336*, 177.
(38) Luo, R.; Head, M. S.; Moult, J.; Gilson, M. K. *J. Am. Chem. Soc.* **1998**, *120*, 6138.
(39) Lim, C.; Bashford, D.; Karplus, M. *J. Phys. Chem.* **1991**, *95*, 5610.
(40) Gao, J.; Li, N.; Freinhof, M. *J. Am. Chem. Soc.* **1996**, *118*, 4912.
(41) Winkler, K.; Lindner, J.; Subramaniam, V.; Jovin, T. M.; Vöhringer, P. *Phys. Chem. Chem. Phys.* **2002**, *4*, 1072.
(42) Helms, V.; Winstead, C.; Langhoff, P. W. *THEOCHEM* **2000**, *506*, 179.
(43) Thompson, M. A.; Zerner, M. *J. Am. Chem. Soc.* **1991**, *113*, 8210.
(44) Press, W. H.; Flannery, B. P.; Teukolsky, S. A.; Vetterling, W. T. *Numerical Recipes;* Cambridge University Press: Cambridge, U.K., 1988.
(45) Tozzini, V.; Nifosi, R. *J. Phys. Chem. B* **2001**, *105*, 5797.
(46) Kar, T.; Scheiner, S.; Cuma, M. *J. Chem. Phys.* **1999**, *111*, 849.
(47) Nielsen, S. B.; Lapierre, J. U.; Andersen, J. U.; Pedersen, U. V.; Andersen, L. H. *Phys. Rev. Lett.* **2001**, *87*, 228102-1.
(48) Gutmann, M.; Nachliel, E. *Biochim. Biophys. Acta* **1990**, *1015*, 391.
(49) Burda, C.; Abdel-Kadar, M. H.; Link, S.; El-Sayed, M. A. *J. Am. Chem. Soc.* **2000**, *122*, 6720.
(50) Schellenberg, P.; Johnson, E.; Esposito, A. P.; Reid, P. J.; Parson, W. *J. Phys. Chem. B* **2001**, *105*, 5316.
(51) Steinberg, G.; Ottolenghi, M.; Sheves, M. *Biophys. J.* **1993**, *64*, 1499.
(52) Cramer, C. J. *Essentials of Computational Chemistry*; J. Wiley & Sons: Chichester, U.K., 2002.
(53) Ward, W. W.; Prentice, H. J.; Roth, A. F.; Cody, C. W.; Reeves, S. C. *Photochem. Photobiol.* **1982**, *35*, 803.
(54) Pitzer, K. S.; Gwinn, W. D. *J. Chem. Phys.* **1942**, *10*, 428.
(55) Stübner, M. R.; Schellenberg, P. *J. Phys. Chem. A* **2003**, *107*, 1246.
(56) Song, L.; El-Sayed, M. A. *J. Am. Chem. Soc.* **1998**, *120*, 8889.
(57) Esposito, A. P.; Schellenberg, P.; Parson, W. W.; Reid, P. J. *J. Mol. Struct.* **2001**, *56*9, 25.
(58) Lide, D. R., Ed. *CRC Handbook of Chemistry and Physics*, 79th ed.; CRC Press: Boca Raton, Fl, 1998; pp 8.46−8.56.